# Structured Electron Transfer Transition State. Valence Bond Configuration Mixing Analysis and ab Initio Calculations of the Reactions of Formaldehyde Radical Anion with Methyl Chlo…

**ARTICLE** *in* THE JOURNAL OF PHYSICAL CHEMISTRY · JULY 1996

Impact Factor: 2.78 · DOI: 10.1021/jp952827z



**2 AUTHORS:**

G Narahari Sastry
Indian Institute of Chemical Technology
**262** PUBLICATIONS **5,205** CITATIONS
SEE PROFILE

Sason Shaik
Hebrew University of Jerusalem
**525** PUBLICATIONS **20,528** CITATIONS
SEE PROFILE

# Structured Electron Transfer Transition State. Valence Bond Configuration Mixing Analysis and ab Initio Calculations of the Reactions of Formaldehyde Radical Anion with Methyl Chloride

**G. Narahari Sastry and Sason Shaik***

*Department of Organic Chemistry and the Fritz Haber Center of Molecular Dynamics, The Hebrew University, Jerusalem 91904, Israel*

*Received: September 22, 1995; In Final Form: March 11, 1996*[⊗]

Ab initio computations are performed on the competing electron transfer (ET) and substitution (SUB) pathways between formaldehyde radical anion and methyl chloride. The results are followed by a valence bond configuration mixing (VBCM) analysis. A variety of computational procedures starting from UHF and ROHF, with four different basis sets, on to higher levels up to UQCISD optimization, establish the existence of two transition states (TSs). One having a general $(OH_2C\text{---}CH_3\text{---}Cl)^{\bullet-}$ structure corresponds to the ET pathway, and the other with the general $(CH_2O\text{---}C\text{---}Cl)^{\bullet-}$ structure corresponds to the O-alkylation (SUB(O)) pathway. No TS could be located for the direct C-alkylation pathway, and the C-alkylated product is formed in a stepwise manner. The ET-TS is bonded and has a distinct stereochemistry compared to the analogous SUB-(O)-TS. A detailed path-following study, starting from the ET-TS in the direction of products, shows that the mode with the negative force constant (the reaction vector) along the reaction coordinate changes its character from a C---C approach to a C---C recoil. The recoil is triggered by the flapping mode of the two hydrogens of the formyl group which opposes the C---C approach and directs the final destiny of the path toward dissociative ET. A systematic computational study establishes that the ROHF/6-31G* level is a consistent level for geometry optimization, while a single point calculation UCCSD(T)/6-31+G*//ROHF/6-31G* is sufficient for obtaining reliable energetics. The points along the IRC path at UHF and UMP2 levels are highly spin contaminated and lead to erroneous conclusions when using MW (mass-weighted) coordinates. The mechanistic details and the TS stereochemistries established for the molecular calculations in vacuum persist when the calculations are repeated with the SCRF method based on the simple reaction field solvent model. Orbital selection rules are derived from the VBCM analysis to understand the structural features of ET- and SUB(O)-TSs and also the absence of a TS for the direct C-alkylation pathway. Probes are proposed to test the bonded nature of the ET-TS and its distinct stereochemistry compared with the SUB(O)-TS.

## Introduction

Electron transfer (ET) is a ubiquitous process, which occurs alongside other reactions for radical-anion/alkyl halide reactant pairs.[1−4] Consider, for example, the potential reaction pathways between a typical ketyl radical anion and alkyl halide in Scheme 1. Thus, in addition to a dissociative ET, the radical anion may undergo two substitution (SUB) type reactions: a C-alkylation denoted as SUB(C) and an O-alkylation denoted as SUB(O). Using the language of physical organic chemistry, these latter two processes are termed "polar reactions", and as such Scheme 1 shows the common mechanistic dichotomy between ET and polar processes[5] which is often observed for pairs of reacting nucleophile and electrophile (e.g., the radical anion = nucleophile, and the alkyl halide = electrophile). This dichotomy has been a source of intense activity and lively discussions in the past decade.[1−15]

In a preliminary communication we have reported an ab initio investigation of the reactivity pathways for a model system consisting of a formaldehyde radical anion and methyl chloride.[15a] It was found that the reactants undergo two of the reactions in Scheme 1, dissociative ET and SUB(O), while no evidence could be found for a *direct* SUB(C) starting from the reactants. This computational mechanistic scheme seems to be in accord with findings in analogous experimental systems.[3a,b,16] Furthermore, in the preliminary study it was shown that both ET and SUB(O) processes obey orbital selection rules, and as such the ET-TS has a stereospecific structure that meets the bonding requirements imposed by the selection rule.[15a] These mechanistic and structural results recurred in the preliminary computational investigation of cases where the formyl anion radical was linked to the alkyl halide moiety via $-(CH_2)_n-$ units.[15b] Since good structural data and electronic features of ET-TSs are not ubiquitous, and due to the potential importance of this preliminary result to the field of ET reactivity, it was deemed

**SCHEME 1**

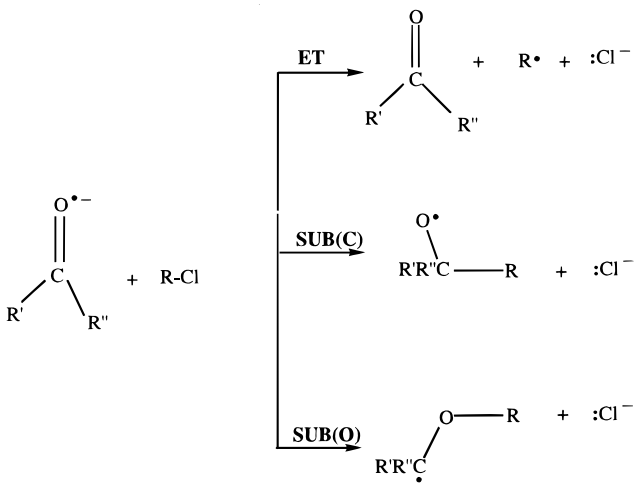


[⊗] Abstract published in *Advance ACS Abstracts,* July 1, 1996.

S0022-3654(95)02827-9 CCC: $12.00 

necessary (i) to benchmark the study, of formaldehyde radical anion reacting with methyl chloride, by estimating the dependence, if any, of the mechanistic conclusions on the choice of method employed and (ii) to analyze the mechanistic findings on the basis of VBCM principles. In doing so, we aim to set computational standards and know-how for locating and identifying bonded ET-TSs[17] and at the same time to form a platform for thinking on the bonding and structural principles of ET-TSs and their relationship to the TSs for the polar reactions, SUB(O) and SUB(C).

## Theoretical Methods and Calculations

All the computations for the model processes in Scheme 1 were performed with the Gaussian 92 program package.[18] In some specified cases we also used the GAMESS-93 package.[19]

Geometry optimization was carried out with various methods. The UHF method is contaminated by states of higher spin multiplicity, and as shall be seen later, this feature of the UHF method creates difficulties for path following and mechanistic assignment of the TSs. In contrast, the ROHF procedure is free of spin contamination, but its energies are higher compared to the UHF procedure. Since it is not a priori clear what is the best procedure for a given problem, optimizations were performed at UHF, ROHF, and UMP2 levels of theory. As the highest geometry optimization level we used UQCISD/6-31G* for locating the ET-TS, the SUB(O)-TS, and the precursor cluster, $C_R$ (see Figure 2 later for labels). Since frequency calculations at UQCISD at present can only be done numerically, which is prohibitively expensive, we had to avoid the frequency calculations. This poses, however, no serious problem since the geometry optimization was performed without any symmetry restrictions, and as such, the resulting UQCISD/6-31G* structures may be designated as genuine critical points.

To examine the sensitivity of the geometries of the critical species and of the central barriers to basis set variations, the calculations were done with an array of basis sets, viz., 3-21G, 6-31G*, 6-31G**, 6-311G*, and 6-31+G*, as well as an ECP/LANL1DZ(2d) valence basis set coupled with the effective core potential of Hay and Wadt[20] and generated from the original LANL1DZ basis set for Cl augmented with two sets of uncontracted d type polarization functions (Cl; $\alpha_d = 0.150$ and 0.375; the 6-31G* basis set was used for C, O, H, and N atoms). Since the key results are virtually the same (see later) for all the basis sets, we shall not show all the data to save space. The barrier heights for the ET and SUB(O) pathways were evaluated by means of single-point calculations at ROMP2,[21] UQCISD(T),[22] and UCCSD(T)[23] levels of theory with the 6-31+G* basis set and all the way up to the UCCSD(T)/6-31++G** level on UQCISD/6-31G* optimized geometries. All the calculations at the correlated levels were performed with the frozen core approximation.

All the species of ET and SUB(O) pathways were characterized by geometry optimization and frequency analysis using the GAUSSIAN 92 routines. Reaction pathways were ascertained by means of the Gonzalez−Schlegel path-following techniques,[24] which are standard computational procedures for assigning a TS to a particular mechanism. The path-following calculations were done at the UHF and ROHF levels with internal coordinates in a **Z**-matrix format[24a] and also with mass-weighted internal coordinates on ET-TS.[24b] IRC path following in Cartesian coordinates at ROHF/6-31G* and UHF/6-31G* levels was done using GAMESS-93[19] and gave identical trends as the internal coordinates. As such, the results of the Cartesian coordinate tests will not be discussed any further. For brevity, the keyword IRC used in the GAUSSIAN manual will be adapted to indicate path following, while in parentheses we shall specify the coordinate system used to follow the path. Thus, IRC(Z-int) indicates that internal coordinates (in a **Z**-matrix format) which are non mass weighted[24a] are used in the path following, while IRC(MW-int) indicates that the calculations are done with mass-weighted[24b] internal coordinates. Path following at the UMP2 level was done only with IRC(Z-int). In a typical situation, the path-following calculations for the ET-TS were carried out until the point where a C···C recoil takes place, leading to a neutral formaldehyde moiety, while the negative charge resides on Cl and the spin on $CH_3$ (see Figure 2). After reaching this point, the default Berny optimization[25] is employed to reach the minimum of the product cluster. As an example, the **Z**-matrices, in the GAUSSIAN input format, of ET-TS structures at UHF/6-31G* and ROHF/6-31G* levels are given in the Appendix.

The reaction vectors of the ET-TS and along the path were drawn with MOLPLT implemented in the GMAESS-93 package.[19]

**Spin Contamination.** The spin contamination of the UHF and UMP2 wave function of the critical species for ET and SUB(O) mechanisms was found to be small ($\langle S^2 \rangle$ 0.76−0.77), as reflected also in the fact that UHF and ROHF lead to very close geometries and energetics (see Table 1). In contrast, UHF and UMP2 pathways connecting the ET-TS to its successor ET product cluster ($C_{ET}$, Figure 2) were found to suffer from significant spin contamination. Thus, it was found that the IRC(MW-int)[24b] path with the UHF and UMP2 method proceeds along heavily spin contaminated regions (e.g., $\langle S^2 \rangle = 0.875$ for UHF/6-31G*) quite early, past the TS. In contrast, the IRC(Z-int)[24a] path proceeds through regions that are much less contaminated. As shall be seen later, the spin contamination along the path creates artifacts in the mechanistic designation, and therefore the IRC(MW-int) technique coupled with unrestricted wave functions *is unreliable* for these kinds of reactions.

Following the ET step, $CH_3$ radical attacks on formaldehyde can take place to generate the O-alkylation and C-alkylation products. The corresponding radical attack TSs possess high spin contamination; $\langle S^2 \rangle$ values are 0.880 ($C_{AT}$-TS) and 0.965 ($O_{AT}$-TS). Spin projection[26] gave, however, consistent trends in accord with higher levels. Since the radical attack process follows the ET step and is not of prime importance in this study, this particular process is reported only at the UCCSD(T)/6-31+G*//UMP2/6-31+G* level (see Figure 3).

**Isotope Effects.** Isotope effects were calculated using Eyring's equation.[27] Vibrational frequencies and entropies were scaled by the factor 0.8929 at the UHF and ROHF levels, while UMP2 frequencies were scaled by a factor of 0.95.

**Solvent Effects.** The TSs for the ET and polar mechanisms were reoptimized at the UHF level with the SCRF procedure, which incorporates the reaction field solvation model.[28] Following recommended procedure, the solute's cavity radius was obtained by adding 0.5 Å to the radius computed for the gas phase structure. Three different dielectric constants are used, viz., 78.5, 36.2, and 8.9, corresponding to the solvents water, acetonitrile, and dichloromethane, respectively at the room temperature. Two basis sets were used: 6-31G* and 6-31+G*. The SCRF/UHF geometry optimization follows the standard procedure, while IRC(Z-int) was used to assign the mechanism in solvents. The ET-TS was verified by the C···C recoil that leads to the dissociative ET process with a neutral formaldehyde and $CH_3^{\bullet}$ and $Cl^-$ fragments. To evaluate central barriers, single-point calculations were done with the SCRF procedure at higher levels, which are denoted by the usual notations, e.g., SCRF/UMP2/6-31+G*//UMP2/6-31+G*, which signifies a

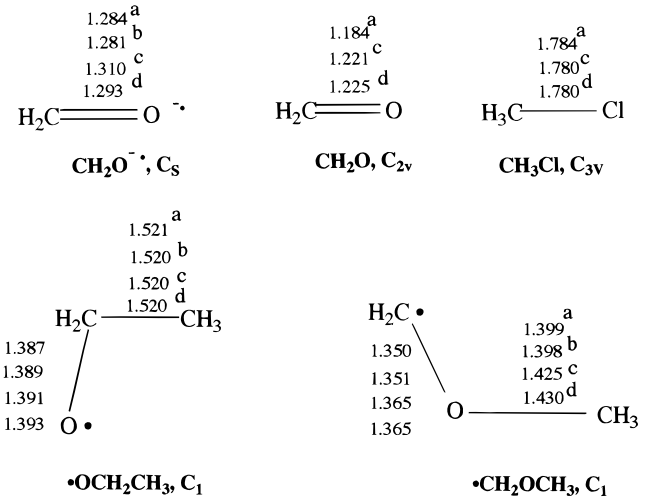


**Figure 1.** Optimized principal bond lengths of $CH_2O^{\bullet-}$, $CH_2O$, $CH_3Cl$, $^{\bullet}OCH_2CH_3$, and $^{\bullet}CH_2OCH_3$, at the (a) UHF/6-31G*, (b) ROHF/6-31G*, (c) UMP2/6-31G*, and (d) UMP2/6-31+G* levels. For the closed shell species a, c, and d represent RHF/6-31G*, RMP2/6-31G*, and RMP2/6-31+G*, respectively. Symmetry labels of the species are indicated.

single-point SCRF calculation at the UMP2 level with the gas-phase UMP2/6-31+G* geometry.

## Results

**A. Mechanistic Details.** *Reactants and Products.* The optimized geometries of the reactants, $CH_2{=}O^{\bullet-}$ and $CH_3Cl$, the ET products, $CH_2{=}O$, and $^{\bullet}CH_3$, the O-alkylation product, $^{\bullet}CH_2OCH_3$, and the C-alkylation product, $^{\bullet}OCH_2CH_3$, are depicted in Figure 1. The spin contamination (in the open shell systems) is small at both the UHF and UMP2 levels, $\langle S^2\rangle$ values being in the range 0.76−0.77. While, the Hartree−Fock levels consistently underestimate the C−O distance in both the anion radical and neutral formaldehyde compared to the UMP2 level, the geometric parameters are virtually identical at the UHF and ROHF levels, and all the levels reproduce the C−O bond shortening in the neutral formaldehyde relative to the radical anion. This bond shortening is a necessary feature of the ET mechanism.

*Transition States (TSs) and Reaction Profiles.* Figure 2 shows the mechanistic scheme verified by both IRC(Z-int) and IRC-(MW-int) techniques at the ROHF level which is free from the spin contamination problem. Full discussions of the IRC nature and other computational levels follow later. The energies in Figure 2 are indicated relative to the separated reactants (defined as the zero of the energy scale). The two mechanisms that are identified in Figure 2 are a dissociative ET via a bonded TS[17] of the general $OCH_2$---$CH_3$---Cl type and SUB(O) via a $CH_2O$---$CH_3$---Cl type TS structure. Both the ET and SUB(O) reaction profiles involve a common precursor cluster, $C_R$, which proceeds to the ET-TS and SUB(O)-TS, which subsequently go on to the product type clusters $C_{ET}$ and $C_{SUB(O)}$, respectively. The product clusters further separate out to the corresponding products ($P_{ET}$, $P_{SUB(O)}$). For the potential SUB(C) mechanism (see Scheme 1) we were unable to find an additional TS with a $OCH_2$---$CH_3$---Cl structure which connects the reactants directly to the C-alkylation cluster and products. Thus, all attempts to locate such a putative structure with C---C distances either shorter or longer than in the ET-TS collapsed to the ET-TS or to the radical attack TS described below in Figure 3. Thus, no TS structure could be located that directly connects $C_R$ to SUB(C) products. These results are in general accord with reports for analogous experimental systems.[3a,b,16]

While C-alkylation does not occur directly in our model system, the respective products may be formed within the ET product cluster, $C_{ET,}$ by $^{\bullet}CH_3$ radical attack on the neutral formaldehyde, $CH_2O$, as shown in Figure 3 which starts from $C_{ET}$ at the center of the diagram. This attack can lead, in turn, to either SUB(C) or SUB(O) products depending on the site of attack. Figure 3 shows that the two processes are essentially $^{\bullet}CH_3$ radical attacks on neutral formaldehyde with $Cl^-$ acting virtually as a spectator group throughout the energy profile. The $^{\bullet}CH_3$ radical attack at the C end of $CH_2O$ is seen to be a facile process compared to the O-end attack, in line with the well-documented experimental and theoretical results.[26a,29] The presence of $Cl^-$ does not seem to alter the picture obtained in its absence. *Therefore, in our model system C-alkylation proceeds via a two-step process involving a single electron transfer to $C_{ET}$ (Figure 2) followed by alkyl radical attack on the neutral formaldehyde.*[30]

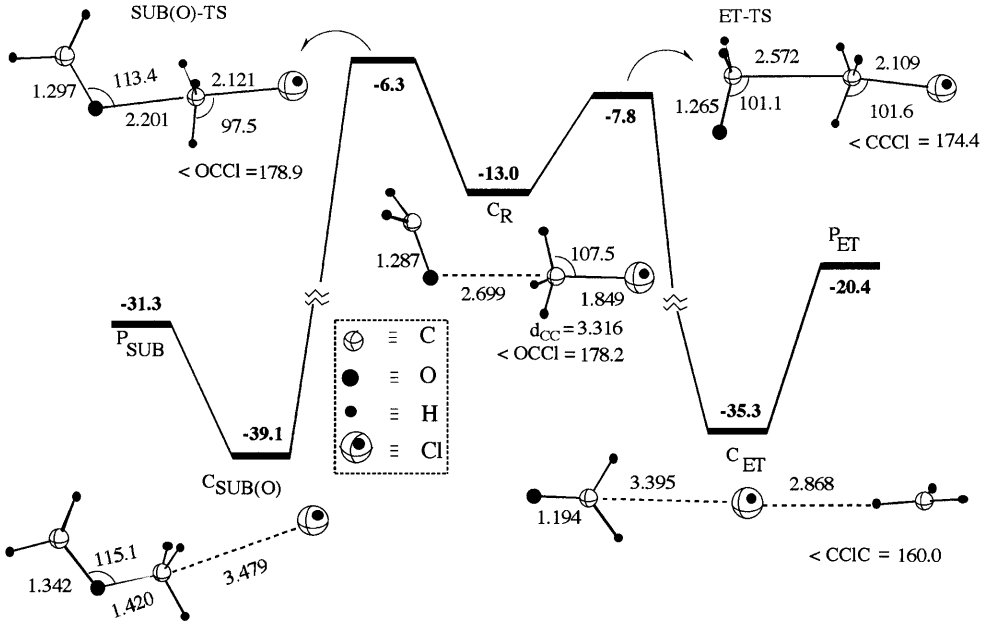


**Figure 2.** UCCSD(T)/6-31+G*//ROHF/6-31G* energy profile for the ET and SUB(O) mechanisms. Profiles are verified by IRC techniques using both IRC-MW as well as IRC(Z-int) coordinates. Energies are given in kcal/mol relative to the reactants.

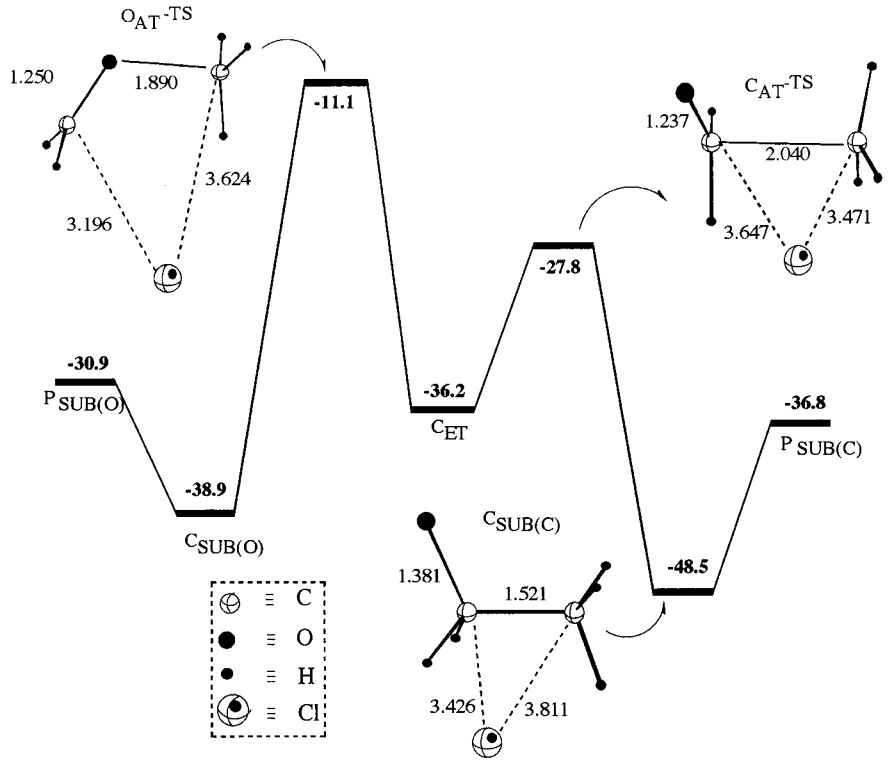


**Figure 3.** UCCSD(T)/6-31+G*//UMP2/6-31+G* energy profile for the $CH_3$ radical attack processes starting within the ET cluster, $C_{ET}$. The energies are in kcal/mol relative to the reactants. The structures of $C_{ET}$ and $C_{SUB(O)}$ refer to Figure 1.

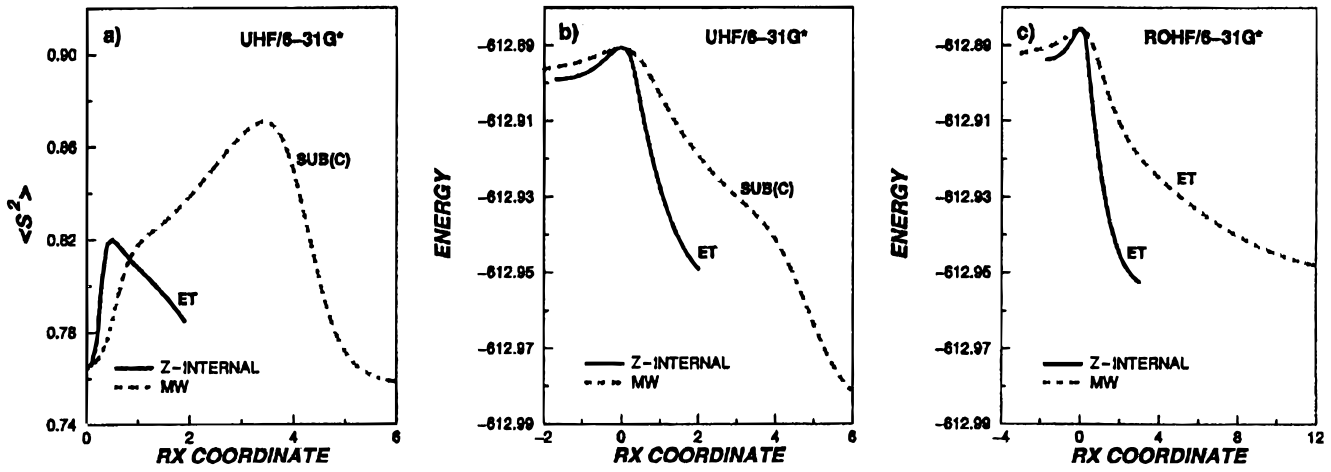


**Figure 4.** Features of IRC(Z-int), denoted as Z-internal, and IRC(MW-int), denoted as MW. (a) $\langle S^2 \rangle$ values along the pathways found by use of the IRC(Z-int) and IRC(MW-int) path-following techniques. Values larger than 0.75 are spin contaminated. (b) Energies along the IRC(Z-int) and IRC(MW-int) paths at UHF/6-31G*. Note the nonsmooth profile along the IRC(MW-int) path. (c) Energies along the IRC(Z-int) and IRC(MW-int) paths at ROHF/6-31G*. Note that now the two profiles are smooth. Energies are in Hartrees, and the reaction coordinate is in $amu^{1/2}$ bohr.

We note that a third TS of the $OCH_2$---Cl---$CH_3$ type, which was located at the UHF and UMP2 levels (with 6-31G* and 6-31+G*), was identified by means of path following as an alternative ET-TS with inverse regiochemistry in comparison with the ET-TS in Figure 2. The $OCH_2$---Cl---$CH_3$ structure was found to be significantly higher in energy than the structure of the type $OCH_2$---$CH_3$---Cl in Figure 2 and was abandoned partly because of significant spin contamination (e.g., $\langle S^2 \rangle$ = 0.836), but chiefly because it could not be located by ROHF theory.

*Path Following and the Nature of the IRC for the ET Mechanism.* Since the ET-TS in Figure 2 is quite unusual, in the sense of being a bonded species with a definitive stereochemistry and specific C---C interaction between the reactants, it was decided to establish by a systematic study how the ET-TS loses ultimately its bonding and dissociates into three fragments (Figure 2). An exhaustive IRC study was therefore undertaken using UHF with different basis sets (3-21G, 6-31G*, 6-31+G*, 6-31G**, 6-311G* and ECP/LANL1DZ(2d)), and UMP2/6-31G*, as well as SCRF/UHF/6-31G*. Finally, the ROHF level which is free from spin contamination was used with a variety of basis sets (6-31G*, 6-31G**, 6-311G*, and 6-31+G* and ECP/LANL1DZ(2d)). In all the UHF and UMP2 cases, IRC(Z-int) assigns the $OCH_2$---$CH_3$---Cl structure as the ET-TS. On the other hand, IRC(MW-int) gave SUB(C) at all these levels. This unusual behavior of the path-following routines[24] was found to originate in the high spin contamination of the IRC(MW-int) path when coupled with the unrestricted UHF and UMP2 methods.

Figure 4a shows the development of the $\langle S^2 \rangle$ value when the $OCH_2$---$CH_3$---Cl type TS is followed down to products along the IRC(Z-int) and IRC(MW-int) paths, using UHF/6-31G* data

which represent general findings for the other unrestricted UHF and UMP2 levels. It is seen that the IRC(MW-int) path is highly spin contaminated, reaching an $\langle S^2 \rangle$ value of 0.875 when the reaction coordinate[24] value reaches 2.5−4.0 amu$^{1/2}$ bohr. Around this region, the TS structure was found to change direction from an ET type to SUB(C). A typical structure at this region of the IRC(MW-int) involves a carbonyl C−O bond length of 1.22 Å, almost as in the formaldehyde product of the ET process, and most of the charge transfer (77%) already took place to the $CH_3Cl$ moiety, with the methyl group having a significant radical character. Thus, the structure where the IRC(MW-int) alters its mechanistic nature has in fact a significant ET character, and at the same time frequency analysis shows that the structure possesses also *two imaginary frequencies*. Indeed, subjecting this structure to the default Berny optimization[25] employed in GAUSSIAN program leads to ET products, a result which seems to suggest that the IRC(MW-int) does not follow the actual steepest descent valley. Indeed, Figure 4b shows the energy along the IRCs, and it is apparent that the IRC(MW-int) energy profile is not smooth and has a break around 2.5−4.0 amu$^{1/2}$ bohr, precisely where the spin contamination peaks along the reaction coordinate. In contrast, the IRC(Z-int) path is well behaved, having relatively small spin contamination (Figure 4a) and a smooth energy profile (Figure 4b). Moreover, it is apparent that the IRC(Z-int) profile has lower energy than IRC(MW-int) at all matching points along the reaction coordinate. These features show that the IRC(MW-int) *is not reliable* and goes astray due to spin contamination along the pathway and that in any event IRC(Z-int) produces the steepest descent pathway leading the $OCH_2$---$CH_3$---Cl structures to dissociative ET products.

To further validate this conclusion, IRC(Z-int) and IRC(MW-int) studies were performed at the ROHF level which is free of spin contamination, using five different basis sets (see above). In all of these cases, *without exception*, both IRC(Z-int) and IRC(MW-int) led the $OCH_2$---$CH_3$---Cl type structure to dissociative ET. Figure 4c shows the energies along the two IRC's for the ROHF/6-31G* level. It is seen first that when no spin contamination interferes, the IRC(MW-int) energy profile is smooth and leads to ET products. Secondly, it is apparent that IRC(Z-int) provides in any case the steepest descent pathway to the same ET product. It follows, therefore, that *the ROHF studies of IRC(MW-int) and IRC(Z-int) validate the ET nature of the process, and at the same time they demonstrate also the validity of the IRC(Z-int) conclusion at the UHF and UMP2 levels that structure of the $OH_2C$---$CH_3$---Cl nature is an ET-TS leading to dissociative ET.*

*The Recoil Mechanism for the ET-TS.* Having established the nature of the bonded ET-TS, it is instructive to consider the reaction coordinate in order to understand how a bonded species, such as the $OCH_2$---$CH_3$---Cl ET-TS can nevertheless recoil to give dissociative ET products. Figure 5 shows the mode with the negative force constant (the reaction vector) for the ET-TS at the UHF, ROHF, and UMP2 levels with different basis sets. The vectors depicted in Figure 5 (also in Figure 6), obtained by the MOLPLT program interfaced to the GAMESS[19] package, display the motions of atoms at the TS along the reaction coordinate in mass-weighted Cartesian coordinates. All the levels in Figure 6 as well as those not included in Figure 6 yield virtually the same vector type. The main features of the vector are its two mutually opposing motions. One is the motion that involves the C---C bond approach with Cl departure. The other is the motion of the two hydrogens of the formyl unit, which perform a flapping movement that opposes the C---C approach. This complex motion is unusual and characteristic of the ET-TS, and this is the motion that triggers the eventual C---C recoil and the resulting dissociative ET. Thus, the hydrogen flapping movement flattens the potential energy in the direction of the initial C---C bond making, and consequently along the reaction coordinate the nature of the reaction vector changes to C---C recoil synchronized with Cl departure. By following the frequencies of the structures along the IRC,[31] one could clearly see this mode interchange occurring very near the ET-TS.

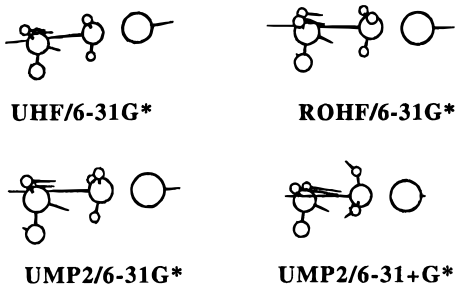


**Figure 5.** Drawings (using MOLPLT routine[19]) of the reaction vectors (the mode with negative force constant) for the ET-TS at different levels. Note the flapping mode of the formyl hydrogens in opposition to the C→ ←C approach movement.

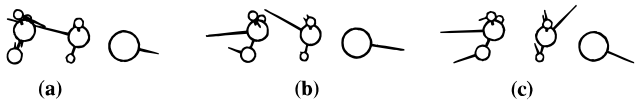


**Figure 6.** Snapshots of the recoil mechanism of the bonded ET-TS. Shown are the changes in the mode with the negative force constant along the IRC(Z-int) pathway at ROHF/6-31G*, starting at (a) with the mode at the TS itself. The same trends are noted with IRC(MW-int) in ROHF/6-31G* and IRC(Z-int) at UHF/6-31G* and UMP2-6-31G*.

Figure 6 shows three snapshots of the reaction vector along the IRC(Z-int) at the ROHF/6-31G* level, which is representative of other tests.[31] Moving from left to right, we see initially at (a) the TS vector with the opposition between the C---C approach and hydrogen flapping modes. As the Cl fragment departs slightly (by 0.083 Å) and the carbonyl C−O bond shrinks a little (by 0.029 Å), while the C---C bond hardly shrinks (by 0.024 Å) relative to its length in the TS, the vector changes its nature to the motion shown in part b of Figure 6, which is seen to involve already a C---C recoil character. Finally, at the right-hand side, drawing c, when Cl departs further (by 0.089 Å) and C−O shrinks still slightly more (by 0.018 Å), the C---C distance starts elongating (by 0.073 Å), and the motion itself is clearly dissociative, leading the $CH_3$ fragment off-axis, while the formaldehyde molecule and $Cl^-$ fly sideways. All these changes occur near the ET-TS, and rather small movements are needed to establish the C---C recoil and dissociative nature of the process. This translation of the hydrogen flapping to a recoil mode of the three particles ($H_2C{=}O$, $CH_3$, $Cl^-$) is associated with momentum transfer between modes and will certainly have interesting dynamic consequences. From our point of view, which is static, the observation of this particular H movement is a telltale sign of an ET process that proceeds via a bonded ET-TS.

**B. A Systematic Study of TS Geometries and Energies.** To benchmark the sensitivity of the geometries and energies of the critical structures and to find the computational level that is minimally demanding in terms of CPU but at the same time also reliable for describing the ET and SUB(O) mechanisms (in Figure 2), we carried out a systematic study at different basis sets and correlation levels.

**TABLE 1: Principal Skeletal Parameters (Å) at the Various Levels of Theory of Some Critical Species on the Energy Profile in Figure 2 (C(1) Corresponds to Formaldehyde's Carbon and C(2) Corresponds to Methyl Chloride's Carbon)**

| level | C(1)−O | C(2)−Cl | C(1)−C(2) | C(2)−O |
|---|---|---|---|---|
| | | $C_R$ | | |
| UHF/6-31G* | 1.290 | 1.847 | 3.324 | 2.715 |
| UHF/6-31G** | 1.290 | 1.847 | 3.308 | 2.704 |
| UHF/6-311G* | 1.289 | 1.855 | 3.347 | 2.716 |
| UHF/6-31+G* | 1.284 | 1.840 | 3.633 | 2.761 |
| ROHF/6-31G* | 1.287 | 1.849 | 3.316 | 2.619 |
| ROHF/6-31G** | 1.288 | 1.849 | 3.295 | 2.691 |
| ROHF/6-311G* | 1.282 | 1.857 | 3.317 | 2.617 |
| ROHF/6-31+G* | 1.277 | 1.840 | 3.594 | 2.754 |
| UMP2/6-31G* | 1.314 | 1.825 | 3.157 | 2.666 |
| UMP2/6-31+G* | 1.301 | 1.847 | 3.456 | 2.695 |
| UQCISD/6-31G* | 1.314 | 1.838 | 3.189 | 2.670 |
| | | ET-TS | | |
| UHF/6-31G* | 1.269 | 2.073 | 2.563 | 3.090 |
| UHF/6-31G** | 1.269 | 2.076 | 2.562 | 3.081 |
| UHF/6-311G* | 1.265 | 2.080 | 2.591 | 3.095 |
| UHF/6-31+G* | 1.269 | 2.101 | 2.563 | 3.122 |
| ROHF/6-31G* | 1.265 | 2.081 | 2.565 | 3.061 |
| ROHF/6-31G** | 1.265 | 2.076 | 2.571 | 3.068 |
| ROHF/6-311G* | 1.260 | 2.081 | 2.601 | 3.075 |
| ROHF/6-31+G* | 1.263 | 2.104 | 2.582 | 3.109 |
| UMP2/6-31G* | 1.293 | 1.990 | 2.541 | 3.042 |
| UMP2/6-31+G* | 1.290 | 2.013 | 2.521 | 3.076 |
| UQCISD/6-31G* | 1.292 | 1.975 | 2.675 | 3.131 |
| | | SUB(O)-TS | | |
| UHF/6-31G* | 1.296 | 2.121 | 2.960 | 2.195 |
| UHF/6-31G** | 1.298 | 2.130 | 2.960 | 2.195 |
| UHF/6-311G* | 1.295 | 2.134 | 2.982 | 2.196 |
| UHF/6-31+G* | 1.297 | 2.181 | 2.973 | 2.156 |
| ROHF/6-31G* | 1.298 | 2.127 | 2.965 | 2.202 |
| ROHF/6-31G** | 1.297 | 2.125 | 2.966 | 2.201 |
| ROHF/6-311G* | 1.293 | 2.131 | 2.988 | 2.201 |
| ROHF/6-31+G* | 1.293 | 2.186 | 2.981 | 2.155 |
| UMP2/6-31G* | 1.325 | 2.094 | 2.818 | 2.116 |
| UMP2/6-31+G* | 1.324 | 2.151 | 2.803 | 2.060 |
| UQCISD/6-31G* | 1.327 | 2.112 | 2.850 | 2.156 |
| | | $C_{ET}$ | | |
| UHF/6-31G* | 1.194 | 4.591 | 7.062 | 8.211 |
| ROHF/6-31G* | 1.194 | 3.939 | 7.058 | 8.201 |
| UMP2/6-31G* | 1.229 | 3.737 | 6.348 | 7.441 |
| UMP2/6-31+G* | 1.234 | 3.749 | 6.371 | 7.471 |
| | | $C_{SUB(O)}$ | | |
| UHF/6-31G* | 1.342 | 3.476 | 2.334 | 1.421 |
| ROHF/6-31G* | 1.342 | 3.479 | 2.332 | 1.420 |
| UMP2/6-31G* | 1.356 | 3.283 | 2.345 | 1.450 |
| UMP2/6-31+G* | 1.356 | 3.347 | 2.354 | 1.454 |

*Geometries.* Table 1 provides the principal skeletal parameters of the critical species of Figure 2 at different levels of geometry optimization. At the highest level, UQCISD/6-31G*, only the three principal structures of Figure 2, $C_R$, ET-TS, and SUB(O)-TS, were optimized. The first notable trend is the consistency of the UHF and ROHF levels for a given basis set. Thus, by and large, the SCF levels provide an internally consistent structural picture independent of the restricted or unrestricted nature of the SCF procedure. In comparison with the higher levels, both UHF and ROHF underestimate the carbonyl's C−O bond length of the cluster $C_R$ and the ET-TS, much as was noted above for the formaldehyde and its radical anion (Figure 1). Another comparison concerns the intermolecular distances in the two TSs. In this respect, the UMP2 level slightly tightens the $C_1$---$C_2$ intermolecular distance in the ET-TS in comparison with UHF and ROHF, while the UQCISD level slightly elongates this distance. As such, the HF geometries are closer than the UMP2 geoemtries to the benchmark method, UQCISD. In contrast, for the SUB(O)-TS both UMP2 and UQCISD tighten slightly the $C_2$---O in comparison with UHF and ROHF.

The effects of basis sets on the geometries seem to be small and not crucial. Thus, relative to the 6-31G* basis set, neither polarization functions on the hydrogens (6-31G**) nor the increase of the degree of splitting of the valence orbitals (6-311G*) seems to have any major structural impact on the three principal structures $C_R$, ET-TS, and SUB(O)-TS. On the other hand, adding diffuse functions to the basis set (6-31+G*) elongates the intermolecular distances in the $C_R$ cluster, as might be expected. On the whole, the structural picture of the TSs seems to be consistent with no major fluctuations and to be reliable at the HF levels with moderate basis sets.

*Gas Phase Energetics.* Table 2 gives the energies of the critical points relative to the reactants at various levels at two basis sets. For a given basis set, the relative energies are virtually identical at the UHF and ROHF levels, as represented by the data in the first two columns. The exothermicities of both ET and SUB(O) reactions are overestimated at the UHF and ROHF levels. The stabilization energies for the reactant cluster are overestimated with the 6-31G* basis set at any level. The additional diffuse functions in 6-31+G* decreased the magnitude of the stabilization energies and gave consistent clustering energies at all levels from UMP2 onward. For the SUB(O) and ET mechanisms the relative trend of the barriers at HF levels is reversed in the post-HF levels, but the absolute values of the barriers remain close for the two mechanisms. All the post-HF methods starting from UMP2 to UCCSD(T) gave the same trends of relative central barriers for the two mechanisms.

The dependence of the relative barriers of ET and SUB(O) on the computational level is seen in Table 3, which collects the central barriers for the two processes. Hartree−Fock levels (UHF and ROHF) consistently overestimate the central barrier for the ET process compared to SUB(O), and the relative trend of the central barriers is identical in all the basis sets employed, 6-31G*, 6-31G**, 6-311G*, and 6-31+G*, at the two HF levels. Thus, there is no apparent basis set effect on the relative barrier heights. In contrast, all the correlated levels from UMP2 onward give a consistent picture that ET has a lower barrier compared to SUB(O). At the UCCSD(T) level of theory the changes in

**TABLE 2: Relative Energies (kcal/mol) of All the Points Shown in Figure 1**

| species | UHF[a] | ROHF[a] | UMP2[a] | UMP2[b,c] | ROHF[b,d] | ROMP2[b,d] | UCCSD(T)[b,c] | UCCSD(T)[b,d] |
|---|---|---|---|---|---|---|---|---|
| reactants | 0.0 | 0.0 | 0.0 | 0.0 | 0.0 | 0.0 | 0.0 | 0.0 |
| $C_R$ | −14.8 | −14.9 | −16.8 | −12.6 | −12.0 | −12.2 | −13.1 | −13.0 |
| ET-TS | −9.1 | −9.4 | −14.0 | −5.5 | −3.3 | −5.7 | −7.9 | −7.8 |
| $C_{ET}$ | −62.2 | −62.9 | −48.1 | −35.1 | −55.0 | −32.7 | −36.1 | −35.3 |
| SUB(O)-TS | −10.6 | −11.0 | −12.0 | −3.8 | − 5.9 | − 3.9 | −5.9 | −6.3 |
| $C_{SUB(O)}$ | −61.1 | −62.2 | −50.2 | −37.3 | −53.8 | − 36.4 | −39.1 | −39.1 |
| $P_{ET}$ | −47.2 | −48.0 | −31.9 | −20.1 | − 41.5 | − 25.2 | −21.1 | −20.4 |
| $P_{SUB(O)}$ | −54.5 | −55.9 | −41.8 | −30.5 | − 48.0 | − 36.0 | −30.9 | −31.3 |

[a] The data correspond to the 6-31G* basis set, and the geometrries are optimized at the same level. [b] The data correspond to the 6-31+G* basis set. [c] Geometries are optimized at the UMP2/6-31+G* level. [d] Geometries are optimized at the ROHF/6-31G* level.

**TABLE 3: Central Barriers (kcal/mol) for ET and SUB(O) Processes**

| level | | | |
|---|---|---|---|
| energy | structure | ET | SUB(O) |
| (1) UHF/6-31G* | UHF/6-31G* | 5.7 | 4.2 |
| (2) UHF/6-31G** | UHF/6-31G** | 5.7 | 4.2 |
| (3) UHF/6-311G* | UHF/6-311G* | 6.2 | 3.9 |
| (4) UHF/6-31+G* | UHF/6-31+G* | 9.4 | 6.9 |
| (5) ROHF/6-31G* | ROHF/6-31G* | 5.5 | 3.9 |
| (6) ROHF/6-31G** | ROHF/6-31G** | 5.5 | 3.9 |
| (7) ROHF/6-311G* | ROHF/6-311G* | 6.0 | 3.9 |
| (8) ROHF/6-31+G* | ROHF/6-31+G* | 9.6 | 7.0 |
| (9) UMP2/6-31G* | UMP2/6-31G* | 2.8 | 4.8 |
| (10) UMP2/6-31+G* | UMP2/6-31+G* | 7.2 | 8.9 |
| (11)UQCISD/6-31G* | UQCISD/6-31G* | 1.5 | 4.3 |
| (12) ROMP2/6-31+G* | UMP2/6-31+G* | 6.8 | 9.6 |
| (13)UQCISD/6-31+G* | UMP2/6-31+G* | 6.4 | 8.4 |
| (14)UQCISD(T)/6-31+G* | UMP2/6-31+G* | 5.3 | 7.2 |
| (15)UCCSD/6-31+G* | UMP2/6-31+G* | 6.8 | 8.9 |
| (16)UCCSD(T)/6-31+G* | UMP2/6-31+G* | 5.5 | 7.6 |
| (17)UCCSD/6-31+G* | UMP2/6-31G* | 5.3 | 6.9 |
| (18)UCCSD(T)/6-31+G* | UHF/6-31G* | 4.7 | 6.4 |
| (19)UCCSD(T)/6-31+G* | ROHF/6-31G* | 5.2 | 6.8 |
| (20)UCCSD/6-31+G* | UQCISD/6-31G* | 4.2 | 6.3 |
| (21)UCCSD(T)/6-31+G* | UQCISD/6-31G* | 5.0 | 7.5 |
| (22)UCCSD/6-31++G** | UQCISD/6-31G* | 4.7 | 7.6 |
| (23)UCCSD(T)/6-31++G** | UQCISD/6-31G* | 3.9 | 6.5 |

the barriers are small going from the 6-31+G* basis set to the 6-31++G** basis set, and one may conclude that the 6-31+G* basis set is sufficient to give reliable energetics for the process.

To ascertain the geometry optimization level, with the least CPU demand, which is reliable for subsequent single-point calculations at higher levels, the central barriers were calculated at the UCCSD(T)/6-31+G* level at geometries corresponding to UHF/6-31G*, ROHF/6-31G*, UMP2/6-31G*, and UMP2/6-31+G* levels (entries 16−19, Table 3). All the combinations gave the same trends and also close absolute magnitudes of the relative barriers heights for both processes. Furthermore, the central barriers at these levels are very close to UCCSD(T)/6-31+G*//UQCISD/6-31G* values. It follows therefore, that ROHF/6-31G* geometry can be taken as a consistent geometry optimization level that provides good energetic trends on subsequent single-point calculations at higher levels using the 6-31+G* basis set.

*Solution Phase Geometries and Energetics.* The TSs for ET and SUB(O) processes were reoptimized and characterized by frequency analysis and IRC path following using the SCRF method in three solvents with dielectric constants corresponding to water, dichloromethane ($CH_2Cl_2$), and acetonitrile ($CH_3CN$). SCRF is a primitive solvent model which nevertheless provides the effect exerted on the molecular system by a dipole perturbation (due to the induction of a dipole in the dielectric).

The mechanistic details are identical in the three solvents, which are in turn identical to the gas phase results: only two TS structures could be relocated corresponding to ET and SUB-(O) processes. No direct C-alkylation could be found with any of the three solvents used in the study as may be judged from the C---C recoil past the ET-TS during the IRC(Z-int)[24a] procedure. The important skeletal parameters of SCRF/UHF/6-31G* and SCRF/UHF/6-31+G* optimized parameters are depicted in Figure 7. The geometries and the orientations of the twin TSs at the SCRF/UHF/6-31G* and SCRF/UHF/6-31+G* levels are very close to those in the gas phase, and there is no significant perturbation on the geometric or mechanistic details by introducing the solvent model or even by changing the solvent polarity.

As no precursor clusters could be located on the SCRF potential energy surface, the central barriers in the solution were evaluated relative to the gas phase reactant cluster. The central barriers calculated at the optimization levels SCRF/UHF/6-31G* and SCRF//UHF/6-31+G* in the three solvents and at the single-point SCRF/UMP2 and SCRF/UQCISD levels are given in Table 4. Single-point calculations were done at the UMP2 and UQCISD levels. Much as in the gas phase, here too a correlated level is required to restore the relative order of barriers (ET barrier being smaller). The solvation is seen to increase the difference between the barriers and to create a higher preference for the ET process, especially at the UQCISD/6-31+G* level.

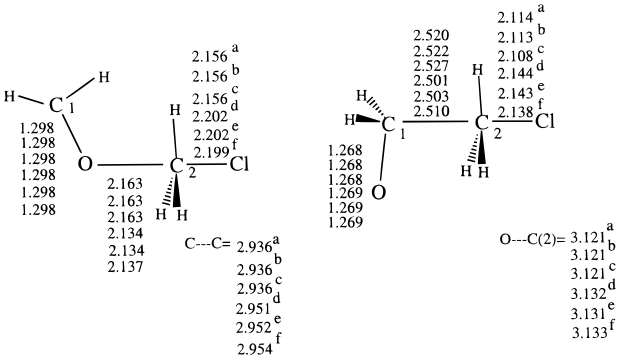


**Figure 7.** SCRF/UHF/6-31G* optimized bond lengths in (a) water, (b) $CH_2Cl_2$, and (c) acetonitrile; SCRF/UHF/6-31+G* optimized values in the same three solvents in d, e, and f.

**TABLE 4: Central Barriers (kcal/mol) for ET and SUB(O) Processes in Solvents[a,b]**

| level | solvent | ET | SUB(O) |
|---|---|---|---|
| (1) SCRF/UHF/6-31G* | water | 5.0 | 4.5 |
| (2) SCRF/UHF/6-31G* | acetonitrile | 4.9 | 4.4 |
| (3) SCRF/UHF/6-31G* | $CH_2Cl_2$ | 4.5 | 3.9 |
| (4) SCRF/UHF/6-31+G* | water | 12.3 | 11.1 |
| (5) SCRF/UHF/6-31+G* | acetonitrile | 12.3 | 11.1 |
| (6) SCRF/UHF/6-31+G* | $CH_2Cl_2$ | 11.9 | 10.5 |
| (7) SCRF/UMP2/6-31G*// UMP2/6-31 | water | 5.0 | 8.6 |
| (8) SCRF/UMP2/6-31G*// UMP2/6-31 | acetonitrile | 4.9 | 8.5 |
| (9) SCRF/UMP2/6-31G*// UMP2/6-31G* | $CH_2Cl_2$ | 4.6 | 8.0 |
| (10) SCRF/UMP2/6-31+G*// UMP2/6-31+G* | water | 10.8 | 14.8 |
| (11) SCRF/UMP2/6-31+G*// UMP2/6-31+G* | acetonitrile | 10.7 | 14.7 |
| (12) SCRF/UMP2/6-31+G*// UMP2/6-31+G* | $CH_2Cl_2$ | 10.1 | 13.7 |
| (13) SCRF/UQCISD/6-31G*// UQCISD/6-31G* | water | 4.6 | 9.4 |
| (14) SCRF/UQCISD/6-31+G*// UQCISD/6-31G* | water | 5.3 | 11.0 |

[a] In entries 1−6 the structures are optimized at the corresponding SCRF/UHF level; for example, entry 4 corresponds to SCRF/UHF/6-31+G*//SCRF/UHF/6-31+G*. [b] Entries 7−14 refer to single point SCRF calculations; for example, entry 14 corresponds to SCRF/UQCISD/6-31+G* single-point calculations on the geometries optimized at the UQCISD/6-31G* level in the gas phase.

## Discussion

The above results raise a few questions. Firstly, what is the origin of the bonding principles that govern the structures of the ET- and SUB-TSs? Second, why was it not possible to find a direct SUB(C)-TS although the corresponding process is the thermodynamically favored one? Third, why does the ET event take place through the C center when the extra charge in

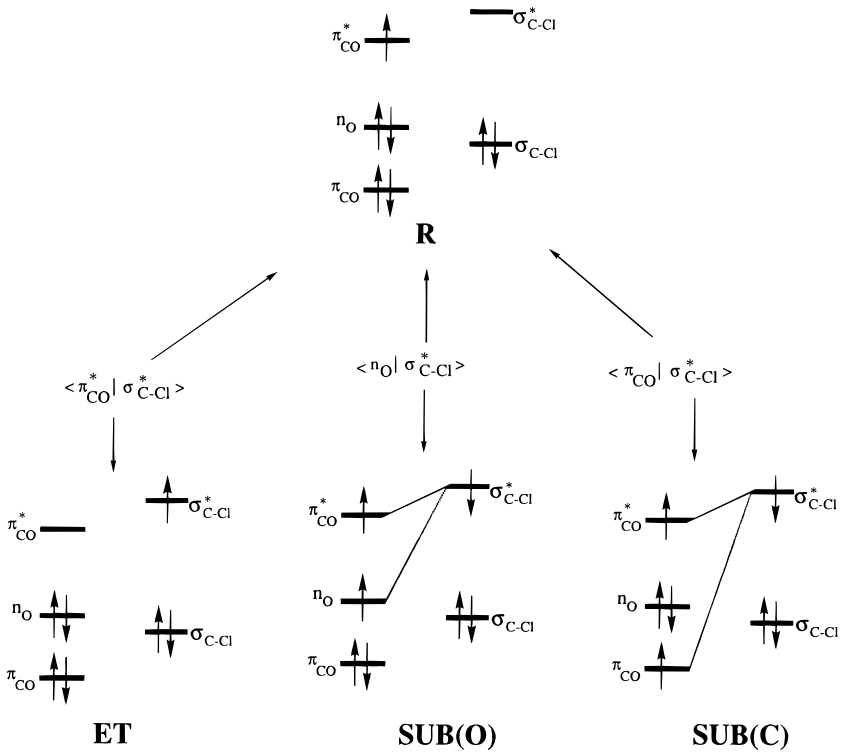


**Figure 8.** Configurations required for VBCM analysis of the ET, SUB(O), and SUB(C) processes. The mixing patterns are shown by the overlap integrals near the arrows that connect the **R** configuration to each of the excited configurations. Orbital selection rules for the TS structure follow these overlaps.

the formaldehyde anion radical resides on oxygen?[32] Since the oxygen is already ligated to the carbon atom of methyl chloride in the cluster $C_R$ (Figure 2), the major structural change to a $OH_2C$---$CH_3$---Cl arrangement at the ET-TS indicates that the ET-TS has a specific bonding requirement, which we wish to understand.

**A. Valence Bond Configuration Mixing (VBCM) Analysis.** *Orbital Selection Rules for ET and SUB(O) Processes.* The VBCM Method can provide insight into the structure of the TS that is possible for a given mechanism by focusing on the bonding properties of the contributing key VB structures and their mixing patterns.[33] Figure 8 shows the minimal number of VB configurations that are important for conceptualizing the mechanisms in Scheme 1.[8] The VB configurations distribute the seven active electrons in reactant fragment MOs, which themselves are not frozen and involve adaptation to the geometric changes along the reaction coordinate. Thus, the first configuration labeled **R** stands for the reactant configuration, where the electrons occupy the orbitals as in the reactant state. To induce any chemical change in the reactants and their bonding patterns, we must mix into **R** additional configurations with different electron population and pairing properties than **R**. These configurations are generated, in turn, by excitations within the orbitals in **R**, and the lowest such excitations give rise to the three configurations **ET**, **SUB(O)**, and **SUB(C)**, which are designated as such due to their ultimate characters as descriptors of the products of the respective processes. The bonding features of these latter configurations and their mixing patterns with **R** provide structural selection rules for the corresponding processes.

The two SUB configurations require some explanations. In both cases there exist three unpaired electrons that are coupled into a total doublet state and provide thereby the new intermolecular bond between the two reactant moieties.[8] In the case of **SUB(O)** the neutral carbonyl fragment is in an $^3n\pi^*$ situation. Since the $^3n\pi^*$ configuration of $H_2CO$ is described mainly by

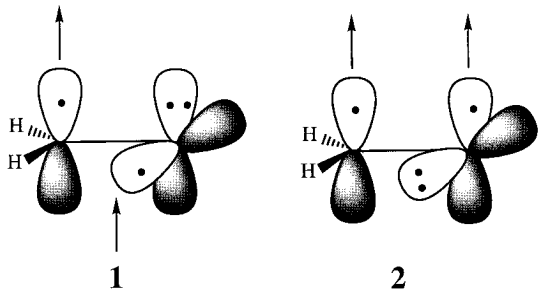

**1** **2**

VB structure **1**, the doublet coupling of the two unpaired electrons to the $\sigma^*_{C-Cl}$ electron to form the new intermolecular bond can be achieved through either C or O centers, but in different planes of the formaldehyde. In the case of **SUB(C)** the neutral carbonyl is in its $^3\pi\pi^*$ configuration and is coupled to the $\sigma^*_{C-Cl}$ electron to a total doublet spin. Since the $^3\pi\pi^*$ state is simply **2**, the new intermolecular bond can be made either through the oxygen or through the carbon in the same plane of the formaldehyde. The decisive factor that will determine the orientation and regioselection of the bond making between the reacting fragments is the resonance interaction of **SUB(O)** and **SUB(C)** with the reactant's configuration, **R**. The **ET** configuration per se has no intrinsic ability to make a new intermolecular bond, and therefore the structure of the ET-TS will be controlled fully by the resonance interaction due to the mixing of **ET** with **R**.

According to the VBCM analysis,[33] the resonance mixing interaction between **SUB(O)** and **R** (Figure 8) requires the optimization of the intermolecular overlap between the orbitals $\sigma^*_{C-Cl}$ and $n_O$. Consequently, the SUB(O)-TS will be stabilized most efficiently by O--C--Cl bonding type, where the formaldehyde moiety approaches in plane, as shown in the overlap cartoon in **3**. It is apparent that this is precisely the orientation and regioselectivity that result from all the computational levels (Figures 2 and 7).

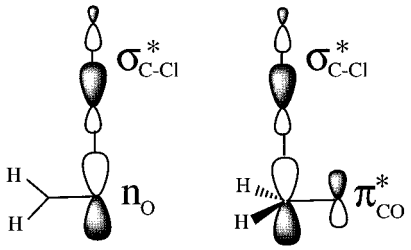


**3** **4**

The resonance interaction between **ET** and **R** (Figure 8) requires the optimization of the overlap between $\pi^*_{CO}$ and $\sigma^*_{C-Cl}$. As shown in **4**, the predicted structure of the ET-TS involves $OH_2C$---$CH_3$---Cl type bonding where now the formaldehyde moiety approaches in its $\pi$-plane and the bonding is established through the carbonyl carbon due to the larger $\pi^*_{CO}$ coefficient on this site. Once again this structural prediction is corroborated by the computed ab initio structure (Figures 2 and 7). It appears, therefore, that the orbital selection rules (due to the resonance interactions) endow the ET-TS and SUB(O)-TS with specific and unique bonding features that determine the stereochemical characteristics of these two TSs. The role of orbital interactions in ET-TSs has been emphasized before by Lund and co-workers;[2a,b] our VBCM analysis highlights the specificity of these bonding requirements.

*Orbital Selection Rule for SUB(C)-TS and Its Competition with ET-TS.* Let us turn now to the resonance mixing for the putative SUB(C)-TS for C-alkylation. VBCM analysis shows that the resonance interaction between **SUB(C)** and **R** (Figure 8) requires optimization of the overlap between $\pi_{CO}$ and $\sigma^*_{C-Cl}$. Since $\pi_{CO}$ has the larger coefficient on the oxygen, the optimization condition will prefer O- - -C- - -Cl bonding, which obviously does not lead to C-alkylation. A less favorable resonance interaction does exist via the smaller $\pi_{CO}$ coefficient in a C- - -C- - -Cl bonding type. *Thus, the C-alkylation is the only reaction among the three options that does not possess a mechanism to optimize its TS bonding.*

Moreover, along the C- - -C- - -Cl trajectory, not only does the putative SUB(C)-TS have to compromise for a lesser bonding but it must also compete with the ET-TS that optimizes its energy along the C- - -C- - -Cl trajectory. Since *the ET-TS is of the bonded type*, it follows that the SUB(C)-TS and ET-TS must be achieved along virtually similar C---C---Cl arrangements (note however the vectors of ET-TS in Figure 5). The lowest of the two structures will occupy the saddle point, while the higher structure of the two will have to be located at the "pommel" or "seat" higher energy regions of the saddle region, in which case the higher structure is not a saddle point. Alternatively the higher energy structure may be relocated altogether to a different region of the C---C---Cl trajectory and be a higher energy saddle point. While we cannot rationalize why our study yields only one saddle point of the given structural type $OCH_2C$---$CH_3$---Cl, we may nevertheless offer a reason based on VBCM analysis for the lower energy of the bonded ET-TS relative to a putative SUB(C)-TS of the same structural type.

The outcome of the ET-TS/SUB(C)-TS competition, and hence also the exclusion of one of these TSs, in our system will be determined by energetic factors. At the reactant geometry, the configuration **R** is the ground state, while all the others are excited states.[8,33] As may be seen from Figure 8, the vertical gap for the ET process involves only charge transfer from $CH_2O^{\bullet-}$ to $CH_3Cl$. The corresponding gap for SUB(C) involves an additional $\pi \rightarrow \pi^*$ excitation, which requires high energy ($\sim$5 eV),[34] and hence the SUB(C) processes will be highly disfavored in terms of the excitation gap factor. On the other hand, ET is modestly disfavored by thermodynamics (by <0.5 eV, see Table 2). Since the barrier is determined by combination of the vertical gap, reaction thermodynamics, and TS resonance energy,[33] we face a situation where the reactivity factors of two reactions clash, and *one expects reactivity crossover* controlled by the donor−acceptor relationship of the reactants.[35] Thus, it is expected[35] that for a good donor−acceptor pair the ET process (with smaller excitation gap) will be favored. On the other hand, for a poorer donor−acceptor pair the SUB(C) process will be favored. While we cannot make a definitive prediction about a single reaction, we nevertheless can rationalize in an educated manner that the absence of SUB(C) in our computations is due to its unfavorable reactivity parameters and to the fact that the $H_2CO^{\bullet-}/CH_3Cl$ is a reasonably good donor−acceptor pair with a significant ET exothermicity. However, since the model predicts reactivity crossover,[35] it is entirely possible that poorer donor−acceptor combinations will favor SUB(C) over ET, as indeed seems to be the case in our preliminary investigation of $YHC{=}O^{\bullet-}/CH_3X$ pairs (Y = H, Me, CN; X = Cl, Br, I).[36]

*The Bonded Character of the ET-TS.* The foregoing discussion indicates clearly that the ET and C-alkylation pathways will be closely related. Thus, since along the $OH_2C$---$CH_3$---Cl trajectory both $\pi^*_{CO}-\sigma^*_{CCl}$ and $\pi_{CO}-\sigma^*_{CCl}$ overlaps coexist, the ET-TS will necessarily mix into its principal configurations **R** and **ET**, also some **SUB(C)** character, and will thereby acquire a multiconfigurational character.

To explore the SUB nature of the ET-TS, we carried out fragment molecular orbital[37] analysis performed directly at the TS geometries, using Slater orbitals. This analysis serves to ascertain the extent of orbital overlap predicted by the VBCM analysis for ET, SUB(C), and SUB(O) pathways (Figure 8). For the SUB(O)-TS the largest overlap (0.072) is $n_O-\sigma^*_{CCl}$, with a negligible contribution from the $\pi^*_{CO}-\sigma^*_{CCl}$ overlap (0.002). Thus, the SUB(O) pathway is controlled almost exclusively by the $n_O-\sigma^*_{CCl}$ interaction and as such behaves effectively like a normal $S_N2$ process possessing a four-electron/three-center TS. At the ET-TS the largest overlap (0.078) is indeed the $\pi^*_{CO}-\sigma^*_{CCl}$ overlap, with zero overlap contribution from $n_O-\sigma^*_{CCl}$. But there is a significant $\pi_{CO}-\sigma^*_{CCl}$ overlap of 0.027. Clearly, though the ET-TS structure is dominated by the $\pi^*_{CO}-\sigma^*_{CCl}$ interaction, it nevertheless involves a significant C-alkylation character. This C-alkylation character in the ET-TS is apparent also from the spin density distribution at various levels. Thus, irrespective of whether these are Mulliken densities at UHF, ROHF, and higher levels up to the projected densities[38] at the UQCISD(T)//UQCISD/6-31G* level or spin densities derived from the Löwdin population[39] analysis (using GMAESS-93[19]), the same trend is obtained: in the ET-TS there is a small but finite accumulation of spin density on the oxygen atom compared with the reactant cluster, $C_R$.[40] This spin density accumulation is typical of a C-alkylation character (see Scheme 1). Thus, in addition to the intrinsic bonding interaction due to the **R**−**ET** configuration mixing, the ET-TS enjoys additional bonding due to the small admixture of the **SUB(C)** configuration. *The availability of a mechanism for optimizing the bonding in the ET-TS constitutes a fundamental energy driving force for the ET reaction to proceed via the bonded ET-TS.*

**B. Structural Probes.** Is it possible to probe and verify by some means the structural features predicted by VBCM analysis and computed by ab initio calculations? To answer the question, we calculated the kinetic isotope effects and entropies of activation for the two mechanisms. The results in Table 5 indicate that the trends in isotope effects are identical at all levels

**TABLE 5: Kinetic Isotope Effects for the Process Corresponding to R → TS**

| | α-$CH_3/CD_3$ | | α-$C^{12/13}$ | |
|---|---|---|---|---|
| level | ET | SUB(O) | ET | SUB(O) |
| UHF/6-31G* | 1.010 | 0.886 | 1.059 | 1.058 |
| UHF/6-31G**[a] | 1.016 | 0.895 | 1.057 | 1.058 |
| UHF/6-311G*[a] | 1.044 | 0.933 | 1.058 | 1.061 |
| UHF/6-31+G*[a] | 1.023 | 0.874 | 1.058 | 1.058 |
| ROHF/6-31G*[a] | 1.009 | 0.891 | 1.059 | 1.060 |
| ROHF/6-31G**[a] | 1.020 | 0.900 | 1.055 | 1.057 |
| ROHF/6-311G*[a] | 1.050 | 0.917 | 1.057 | 1.058 |
| ROHF/6-31+G*[a] | 1.038 | 0.880 | 1.058 | 1.058 |
| UMP2/6-31G*[b] | 1.087 | 0.945 | 1.058 | 1.062 |
| UMP2/6-31+G*[b] | 1.125 | 0.917 | 1.060 | 1.062 |

[a] Frequencies are scaled by a factor of 0.8929. [b] Frequencies are scaled by a factor of 0.95.

of theory. Thus, the α-$C^{12/13}$ isotope effect, which is a measure of the tightness of the TS,[41] has a definitive normal value (Table 5) for both ET and SUB(O) processes, and the magnitudes are comparable to those observed in the experimental $S_N2$ systems. The normal carbon isotope effect for the ET process implies that ET-TS is tightly bonded, much like the analogous SUB-(O)-TS. The α-$CH_3/CD_3$ isotope effect is normal for the ET process and inverse for the SUB(O) process, a trend which is consistently maintained at all levels of theory. It appears, therefore, that in the present model system the α-$CH_3/CD_3$ isotope effect is a mechanistic probe that distinguishes the $OH_2C$---C---Cl bonding of the ET-TS from a putative ET-TS with a $CH_2O$---C---Cl orientation, as well as from the SUB-(O)-TS

Another structural probe is the entropy of activation.[1,2] The $\Delta S^{\ddagger}$ values for each mechanism are independent of the level of calculations employed in this study to within 1 eu. The results show that the ET process is characterized by a large negative entropy of activation (about $-24 \pm 1$ eu for a standard state at 1 M and 298.15 K) comparable to that calculated for the analogous SUB(O) process (about $-26 \pm 1$ eu). The large negative entropy of activation for the ET process indicates that the ET-TS may be structurally akin to their polar analogs and that there is a need for a structural approach to establish the ET-polar dichotomy in anion radical chemistry.

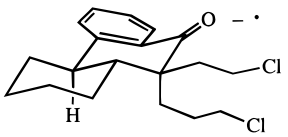


**5**

In this last respect, the orbital selection rules derived in this study impose some well-defined structural requirements that can be tested experimentally by carefully designed systems. The radical anion in **5**, which is a rigid version of the Kimura systems,[3a,b] offers a few such possibilities. Thus, the ketyl anion moiety can react with either the axial or the equatorial alkanyl chloride chains in the α-position to the carbonyl moiety. The equatorial chain is disposed toward an in-plane cyclic TS that involves the $C{=}O^{\bullet-}$ moiety, while the axial chain is more disposed toward a cyclic TS in the $\pi$-plane of the $C{=}O^{\bullet-}$ moiety. According to the orbital selection rules, the SUB(O) mechanism requires an $n_O - \sigma^*_{Cl}$ interaction in the plane of the carbonyl moiety and will therefore take place preferentially via an in-plane oxygen attack on the equatorial chain. In contrast, the ET-TS which requires a $\pi^*_{CO} - \sigma^*_{CCl}$ interaction will take place preferentially via a $\pi$-plane C-attack on the axial chain. The relative reactivities of the two chains can be controlled by changing their lengths, as shown by a recent computational study[15b] of models for the Kimura systems. Thus, an equatorial chain with three $CH_2$ groups will facilitate the SUB(O) process of the chain, while an axial chain with four $CH_2$ groups will facilitate the ET process of this chain. Other changes in this system may involve substitution of the fused benzene ring to modulate the donor property of the $C{=}O^{\bullet-}$ moiety and changes in the halogen to Br and I. A combination of such studies along with the isotope effect probes in Table 5 may help establish the selection rules and especially the specific bonding requirements of the ET-TS.

## Concluding Remarks

The present study uses computational means to benchmark the key features of the ET and SUB mechanisms (Scheme 1) for a model system consisting of a formaldehyde radical anion and a methyl chloride. A variety of computational means revealed two competing mechanisms: O-alkylation (SUB(O)) and ET. The third possible mechanism, the C-alkylation, i.e., SUB(C), was found to occur in a stepwise manner by $CH_3^{\bullet}$ attack on the neutral formaldehyde, past the initial ET step.

From a computational point of view, the study establishes two important points. Firstly, it was shown that spin contamination along the reaction path (even if the TSs themselves are not contaminated) can result in erroneous mechanistic assignment by IRC techniques. This was found to be especially severe when mass-weighted coordinates were used in the IRC procedure at the UHF and UMP2 levels. As such, we recommend carrying out the path following at the ROHF level, which is free of spin contamination and which was found to lead to unequivocal mechanistic assignments independent of the coordinate system. We point out that the pathways generated by means of internal coordinates that are non mass weighted were found to be consistently the steepest descent pathways. Secondly, the ROHF/6-31G* level of theory was established as the least CPU demanding level that is reliable for geometry optimization of the ET-TS and SUB(O)-TS. A single-point calculation on these geometries, UCCSD(T)/6-31+G*//ROHF/6-31G*, gives reliable energetics in accord with higher levels up to UCCSD(T)/6-31+G*//UQCISD/6-31G*.

From a mechanistic point of view, our study establishes the structural features of an *ET-TS that is bonded in a specific manner and that possesses a stereospecific structure* of the type $(OH_2C$---$CH_3$---$Cl)^-$. This is in comparison with the SUB(O)-TS, which has a structure of the $(CH_2O$---$CH_3$---$Cl)^-$ type. The two TSs differ also in the orientation of the formaldehyde moiety, where in ET-TS this moiety is bonded via its $\pi$-plane to the methyl chloride moiety, whereas in SUB(O)-TS the formaldehyde is bonded via the oxygen's lone pair in-plane with the methyl chloride fragment.

A VB mixing analysis is used to derive orbital selection rules that explain the structural features and highlight the specific bonding requirements of the ET-TS. The VB analysis shows also that the ET-TS has a significant admixture of a bond-forming configuration into the principal electronic configurations (**R** and **ET**, in Figure 8), which, in turn, are required by all ET theories.[1,42] The specific bonding requirement of the ET-TS and its multiconfigurational character make it quite unique in the area of ET reactivity. To distinguish this bonded ET-TS from the commonly invoked outer-sphere (weakly bonded) TS, we propose to use the term *structured ET-TS* to describe the type of TSs that possess characteristics similar to the $(OH_2C$---$CH_3$---$Cl)^-$ structure found in this study and in previous studies of related systems.[15b,36] Probes are developed and proposed to test these bonding features as well as the orbital selection rules that account for them.

**Acknowledgment.** This research was sponsored by the Volkswagen Stiftung. The advice of H. B. Schlegel on the IRC issues and projection of frequencies along the path is acknowledged. Discussions with Dinnocenzo about experimental probes for the selection rules are acknowledged. S.S. is thankful for the hospitality at the Department of Chemistry at the University of Rochester.

**CHART 1: Z-Matrix of ET-TS at the ROHF/631G* Level (#ROHF/6-31G* Freq, Electron Transfer Transition State ROHF/6-31G*)**

| | | | | | | | |
|---|---|---|---|---|---|---|---|
| −1 2 | | | | | | | |
| C | | | | | | | |
| O | 1 | r1 | | | | | |
| C | 1 | r2 | 2 | a1 | | | |
| H | 3 | r3 | 1 | a2 | 2 | d1 | 0 |
| Cl | 3 | r4 | 4 | a3 | 1 | d2 | 0 |
| H | 3 | r5 | 1 | a4 | 2 | d3 | 0 |
| H | 3 | r6 | 1 | a5 | 2 | d4 | 0 |
| H | 1 | r7 | 2 | a4 | 3 | d5 | 0 |
| H | 1 | r8 | 2 | a5 | 3 | d6 | 0 |

| | | | |
|---|---|---|---|
| r1 | 1.2651 | a4 | 72.8645 |
| r2 | 2.5716 | a5 | 83.5302 |
| r3 | 1.0662 | a6 | 120.0860 |
| r4 | 2.0724 | a7 | 120.0858 |
| r5 | 1.0658 | d1 | 120.9524 |
| r6 | 1.0662 | d2 | 175.1578 |
| r7 | 1.1070 | d3 | 0.0040 |
| r8 | 1.1070 | d4 | −120.9459 |
| a1 | 101.1439 | d5 | −108.0891 |
| a2 | 83.5328 | d6 | 108.0963 |
| a3 | 99.3047 | | |

**CHART 2: Z-Matrix of ET-TS at the UHF/6-31G* Level (#UHF/6-31G* Freq, Electron Transfer Transition State UHF/6-31G*)**

| | | | | | | | |
|---|---|---|---|---|---|---|---|
| −1 2 | | | | | | | |
| C | | | | | | | |
| O | 1 | r1 | | | | | |
| C | 1 | r2 | 2 | a1 | | | |
| H | 3 | r3 | 1 | a2 | 2 | d1 | 0 |
| Cl | 3 | r4 | 4 | a3 | 1 | d2 | 0 |
| H | 3 | r5 | 1 | a4 | 2 | d3 | 0 |
| H | 3 | r6 | 1 | a5 | 2 | d4 | 0 |
| H | 1 | r7 | 2 | a4 | 3 | d5 | 0 |
| H | 1 | r8 | 2 | a5 | 3 | d6 | 0 |

| | | | |
|---|---|---|---|
| r1 | 1.2693 | a4 | 74.2943 |
| r2 | 2.5632 | a5 | 82.8241 |
| r3 | 1.0659 | a6 | 119.6896 |
| r4 | 2.0727 | a7 | 119.6893 |
| r5 | 1.0654 | d1 | 120.5649 |
| r6 | 1.0659 | d2 | 176.3029 |
| r7 | 1.1065 | d3 | −0.17268 |
| r8 | 1.1065 | d4 | −120.9231 |
| a1 | 102.1311 | d5 | −108.6856 |
| a2 | 82.8244 | d6 | 108.7346 |
| a3 | 99.3328 | | |

## Appendix

Charts 1 and 2 provide coordinates that give complete specification of the ET-TS at two levels. A **Z**-matrix format is used that is the same as the ones used for IRC(Z-int) following. All other data are available from the authors in archive format.

## References and Notes

(1) (a) Eberson, L. *Electron Transfer Reactions in Organic Chemistry*; Springer Verlag: Heidelberg, 1987. (b) Chanon, M. *Bull. Chim. Soc. Fr.* **1982**, *Part II*, 197. (c) Savéant, J.-M. *Adv. Phys. Org. Chem.* **1990**, *26*, 1.

(2) (a) Lund, H.; Daasberg, K.; Lund, T.; Pedersen, S. U. *Acc. Chem. Res.* **1995**, *28*, 313. (b) Daasberg, K.; Pedersen, S. U.; Lund, H. *Acta Chem. Scand.* **1991**, *45*, 424. (c) Daasberg, K.; Christensen, T. B. H. *Acta Chem. Scand.* **1995**, *49*, 128. (d) Simonet, J.; Michel, M.-A.; Lund, H. *Acta Chem. Scand.* **1975**, *B29*, 489. (e) Jorgensen, L. V.; Lund, H. *Acta Chem. Scand.* **1993**, *47*, 577.

(3) (a) Kimura, N.; Takamuku, S. *J. Am. Chem. Soc.* **1994**, *116*, 4087. (b) Kimura, N.; Takamuku, S. *Bull. Chem. Soc. Jpn.* **1991**, *64*, 2433. (c) Kimura, N.; Takamuku, S. *Bull. Chem. Soc. Jpn.* **1993**, *66*, 3613. (d) Kimura, N.; Takamuku, S. *Bull. Chem. Soc. Jpn.* **1992**, *65*, 1668.

(4) (a) Bilkis, I. I. In *The Chemistry of Acid Derivatives*; Patai, S., Ed.; John Wiley: New York, 1992; Vol. 2, p 1639. (b) Bilkis, I. I.; Selivanov, B. A.; Shteingarts, V. D. *Res. Chem. Intermed.* **1993**, *19*, 463.

(5) Pross, A. *Acc. Chem. Res.* **1985**, *18*, 212.

(6) Bank, S.; Noyd, D. A. *J. Am. Chem. Soc.* **1973**, *95*, 8203. (b) Ashby, E. C. *Acc. Chem. Res.* **1988**, *21*, 414. (c) Perrin, C. L. *J. Phys. Chem.* **1984**, *88*, 3611.

(7) (a) Eberson, L. *New J. Chem.* **1992**, *16*, 151. (b) Eberson, L. *J. Chem. Soc., Chem. Commun.* **1975**, 826.

(8) Eberson, L.; Shaik, S. S. *J. Am. Chem. Soc.* **1990**, *112*, 4484.

(9) Lexa, D.; Savéant, J.-M.; Su, K.-B.; Wang, D.-L. *J. Am. Chem. Soc.* **1988**, *110*, 7617.

(10) Schlesener, C. J.; Amatore, C.; Kochi, J. K. *J. Phys. Chem.* **1986**, *40*, 3747.

(11) Julliard, M.; Scagliarini, J. P.; Rajzmann, M.; Chanon, M. *Chimia* **1986**, *40*, 16.

(12) Busli, R. D.; Schwarz, H. *Chem. Ber.* **1990**, *123*, 535.

(13) (a) Kochi, J. K. *Angew. Chem., Int. Ed. Engl.* **1988**, *27*, 1227. (b) For closed shell species the ET-TS is enforced to be outer-sphere; see: (a) Shaik, S. S. *Acta Chem. Scand.* **1990**, *44*, 205. Apeloig, Y.; Aharoni, O. M.; Danovich, D.; Ioffe, A.; Shaik, S. *Isr. J. Chem.* **1993**, *33*, 387.

(14) (a) Reddy, A. C.; Danovich, D.; Ioffe, A.; Shaik, S. *J. Chem. Soc., Perkin Trans. 2* **1995**, 1525. (b) Reddy, A. C.; Sastry, G. N.; Shaik, S. *J. Chem. Soc., Perkin Trans. 2* **1995**, 1717. (c) Cho, J. K.; Shaik, S. S. *J. Am. Chem. Soc.* **1991**, *113*, 9890.

(15) (a) Sastry, G. N.; Shaik, S. *J. Am. Chem. Soc.* **1995**, *117*, 3290. (b) Sastry, G. N.; Reddy, A. C.; Shaik, S. *Angew. Chem.* **1995**, *107*, 1619; *Int. Ed. Engl.* **1995**, *34*, 1495.

(16) (a) Lund, H.; Simmonet, J. *Bull. Soc. Chim. Fr.* **1973**, 1843. (b) Honda, E.; Tokuda, M.; Yoshida, H.; Ogasawara, M. *Bull. Chem. Soc. Jpn.* **1987**, *60*, 851.

(17) Weakly bonded (outer-sphere) ET-TSs may certainly be found. Our recent study of radical cation reactivity (ref 14a) shows that these outer-sphere ET-TSs are generally higher in energy than their bonded analogs. The present study focuses on the bonded TSs, which are interesting from the points of view of bonding principles and the general aim of the paper.

(18) Frisch, M. J.; Trucks, G. W.; Head-Gordon, M.; Gill, P. M. W.; Wong, M. W.; Foresman, J. B.; Johnson, B. G.; Schlegel, H. B.; Robb, M. A.; Replogle, E. S.; Gomperts, R.; Andres, J. L.; Raghavachari, K.; Binkley, J. S.; Gonzalez, C.; Martin, R. L.; Fox, D. J.; Defrees, D. J.; Baker, J.; Stewart, J. J. P.; Pople, J. A. *Gaussian 92, Revision C3*, Gaussian, Inc.: Pittsburgh, PA, 1992.

(19) Schmidt, M. W.; Baldridge, K. K.; Boatz, J. A.; Elbert, S. T.; Gordon, M. S.; Jensen, J. H.; Koseki, S.; Matsunaga, N.; Nguyen, K. A.; Su, S. J.; Windus, T. L.; Dupuis, M.; Montgomery, J. A. *J. Comput. Chem.* **1993**, *14*, 1347.

(20) Hay, P. J.; Wadt, W. R. *J. Chem. Phys.* **1985**, *82*, 270, 299. Wadt, W. R.; Hay, P. J. *J. Chem. Phys.* **1985**, *82*, 284.

(21) Knowles, P. J.; Andrews, J. S.; Amos, R. D.; Handy, N. C.; Pople, J. A. *Chem. Phys. Lett.* **1991**, *186*, 130.

(22) Pople, J. A.; Head-Gordon, M.; Raghavachari, K. *J. Chem. Phys.* **1987**, *87*, 5968.

(23) (a) Scheiner, A. C.; Scuseria, G. E.; Rice, J. E.; Lee, T. J.; Schaefer, H. F. *J. Chem. Phys.* **1987**, *87*, 5361. (b) Bartlett, R. D. *J. Phys. Chem.* **1989**, *93*, 1697.

(24) (a) Gonzalez, C.; Schlegel, H. B. *J. Chem. Phys.* **1989**, *90*, 2154. (b) Gonzalez, C.; Schlegel, H. B. *J. Chem. Phys.* **1990**, *94*, 5523.

(25) Schlegel, H. B. *J. Comput. Chem.* **1982**, *3*, 214.

(26) (a) Gonzalez, C.; Sosa, C.; Schlegel, H. B. *J. Phys. Chem.* **1989**, *93*, 2435. (b) Schlegel, H. B. *J. Phys. Chem.* **1986**, *84*, 4530.

(27) Melander, L.; Saunders, W. H. *Reaction Rates of Isotopic Molecules*; Wiley: New York, 1980.

(28) Wong, M. H.; Frisch, M. J.; Wiberg, K. B. *J. Am. Chem. Soc.* **1991**, *113*, 4776.

(29) Choo, K. Y.; Benson, S. W. *Int. J. Chem. Kinet.* **1981**, *13*, 833.

(30) This is, of course, different than the conditions in solution phase, where the $^{\bullet}CH_3$ radical will most likely couple with the reactant anion radical, which at least initially is present in excess. See ref 4 above.

(31) We have also inspected the projected frequencies orthogonal to the IRC (using iop(7/45=1) in GAUSSIAN-92, as advised by Schlegel, H. B). The combination of the projected and unprojected modes allowed us to ascertain the changes in the modes discussed in Figure 6.

(32) The main VB structure of formaldehyde anion radical is described as $^{\bullet}CH_2O{:}^{-}$, while that of neutral formaldehyde is the covalent and spin-paired structure $^{\bullet}CH_2O^{\bullet}$. Thus, the extra electron on formaldehyde anion radical lies on the O center, and as such the O center might have been considered as the effective electron donor site.

(33) Shaik, S.; Hiberty, P. C. *Adv. Quant. Chem.* **1995**, *26*, 99.

(34) (a) Buenker, B. J.; Peyrimhoff, S. D. *J. Chem. Phys.* **1970**, *53*, 2368. (b) Davis, T. D.; Maggiora, G. M.; Christoffersen, R. E. *J. Am. Chem. Soc.* **1974**, *96*, 7878. (c) Merchan, M.; Roos, B. O. *Theor. Chim. Acta* **1995**, *92*, 227.

(35) Shaik, S. S. *New. J. Chem.* **1982**, *6*, 159 (b) Shaik, S. S. *Prog. Phys. Org. Chem.* **1985**, *15*, 197. The barrier is given in the ususal way by $\Delta E^{\ddagger} = fG - B$ ($G$ is the vertical gap in the avoided crossing diagram, $f$ is the fraction of $G$ that enters under the crossing point, and $B$ is the avoided crossing resonance energy). Since SUB(C) possesses a preferred thermodynamic factor, its respective $f$ value is smaller that that for the ET reaction, which in contrast has a smaller $G$ value. In such a situation it is shown that when $G$ is small, ET will possess the smaller barrier, and vice versa when $G$ is large.

(36) Sastry, G. N.; Danovich, D.; Shaik, S. *Angew. Chem., Int. Ed. Engl.* **1996**, *35*, 1098.

(37) (a) Fujimoto, H.; Hoffmann, R. *J. Phys. Chem.* **1974**, *78*, 1169. (b) Hoffmann, R.; Swenson, T. R.; Wan, C.-C. *J. Am. Chem. Soc.* **1973**, *95*, 7644.

(38) (a) Amos, R. D. *Chem. Phys. Lett.* **1980**, *73*, 602. (b) Wiberg, K. B.; Hadad, C. M.; LePage, T. J.; Breneman, C. M.; Frisch, M. J. *J. Phys. Chem.* **1992**, *96*, 671.

(39) Löwdin, P. O. *J. Chem. Phys.* **1992**, *96*, 671.

(40) The projected UQCISD(T)/6-31G*//UQCISD/6-31G* spin density shows an increase of $0.03e^{-}$ in the spin density on the carbonyl's oxygen atom in the ET-TS in comparison with the $C_R$ cluster. The Löwdin population at ROHF/6-31G* shows an increase of $0.047e^{-}$. In fact, this increase in the spin density on the oxygen atom at the ET-TS relative to the $C_R$ cluster is apparent in all the population analyses used, at all the possible levels studied here.

(41) Axelsson, B. S.; Långsröm, B.; Matsson, O. *J. Am. Chem. Soc.* **1987**, *109*, 7233.

(42) (a) Marcus, R. A. *Annu. Rev. Phys. Chem.* **1964**, *15*, 155. (b) Hush N. S. *J. Chem. Phys.* **1958**, *28*, 962.

JP952827Z